Analytical Analysis of a Dripping Faucet Model based on the Perturbation Method

Ziyang Xu*

Experimental High School Attached to Beijing Normal University, Beijing, China

*Corresponding author: JerryXu2008.C@gmail.com

Abstract

The dripping faucet model is a classical system in fluid mechanics and nonlinear dynamics, and has application value in engineering problems such as inkjet printing and droplet manipulation. Previous studies mostly relied on numerical integration or variational methods to solve the Young–Laplace equation, which leads to high computational cost and makes it difficult to obtain analytical expressions for the hanging drop profile and critical volume. This paper proposes an analytical approximation method based on the perturbation method, used to describe the morphology and stability of a hanging drop at the end of a vertically downward circular thin-walled faucet. Under the condition of small Bond number, a perturbation expansion is applied to the Young–Laplace equation to derive analytical expressions for the hanging drop profile and volume, and a unique critical solution criterion is given based on the convexity of the profile function. In the experiment, a controlled liquid supply system and high-speed photography were used to measure the critical volume of hanging drops under six different faucet inner diameters. The results show that the theoretical predictions are consistent with the experimental results within an error range of 2–12%, and the critical volume increases with faucet radius and Bond number, while being independent of the intrinsic contact angle of the liquid.

Keywords

Interfacial mechanics, perturbation method, dripping faucet, stability analysis, bond number.

1. Introduction

1.1. Research Background

When one end of a pipe is connected to a constant pressure source and the other end is open with a small flow rate, the liquid usually drips from the outlet in the form of discrete droplets. The abstracted system formed in this way is called the dripping faucet model. The dripping faucet model is the foundation of most scientific experiments and is also a challenge in high-precision engineering: in biological and chemical titration and reaction processes, it is necessary to know the error between theoretical exact values and experimental titration results; in the printing industry, the size of ink droplets in inkjet printing determines the sharpness of printed image edges; in the aerospace industry, precise control of the size of fuel droplets ejected from a vehicle nozzle ensures flight safety[10]. This model exhibits many interesting physical properties: the gas–liquid interface profile of the liquid generated at the open end of the faucet and the critical detachment volume are affected by variables such as faucet diameter; at the same time, as the flow rate increases, the interval between droplet drips shows a transition from regular behavior into chaos. The research on the dripping faucet model can mainly be divided into two aspects: one is the quasi-static description of the hanging drop profile and volume at the faucet end, which mostly relies on variational methods or numerical

integration with high computational cost, while this paper proposes an analytical approximation solution based on the perturbation method that can match experimental results with high accuracy; the other is the study of the time-varying problem of droplet growth and dripping. When the water pressure is small, it can be regarded as quasi-static, but when the faucet pressure increases, the dripping speed of droplets increases and gradually enters chaos, and various models have been used in the academic community to classify and capture the transition points and transition forms into chaos.

1.2. Historical Research Results

Since nonlinear dynamics and chaos became important branches of dynamics, the dripping faucet model has remained a classical model in this field, and its study has focused on the chaotic characteristics of dripping intervals under flowing conditions.

Previous research mainly employed the following physical approaches. The first is to construct an oscillation model of the droplet center of mass. The essence of this model is to abandon the explicit expression of how various physical quantities influence the fluid properties of the droplet, in order to explain the time-dependent characteristics of the center-of-mass oscillation with a lower number of degrees of freedom. Martien et al. (1985)[12] first abstracted the droplet dripping pattern as a forced spring oscillator, qualitatively explaining the process by which droplet dripping undergoes period doubling and enters chaos, and preliminarily revealing that the dripping faucet model may be a low-dimensional chaotic system. Sánchez-Ortiz and Salas-Brito (1995)[15] improved Shaw's model, describing the linear relationship between the partial mass of the dripping droplet and the critical impulse, and numerically discovered more complex attractors and hysteresis phenomena. d'Innocenzo and Renna (1996)[6], based on the work of Sánchez and others, introduced viscous dissipation and proposed a liquid bridge recoil model, obtaining analytical solutions and mappings that agree well with experiments. Fuchikami, Ishioka, and Kiyono (1999)[9] introduced partial fluid properties of the droplet into the oscillator model, reflected as nonlinear terms and modulation parameters, thereby achieving better agreement with experimental data. The second approach is to construct a neck breakup model. The "neck" is located at the connection between the dripping part of the droplet and the liquid bridge, and serves as the fracture point when the droplet detaches. A general method for handling this model is to construct a one-dimensional slender flow model including the neck region and solve its Navier–Stokes equation. Eggers and Dupont (1994)[8] and Eggers (1997)[7] pointed out that in an ideal Newtonian liquid, the solution of the Navier–Stokes equation near the breakup point exhibits a self-similar singularity, with the radius shrinking according to a power law over time. Kiyono and Fuchikami (1999)[11], applying Eggers' conclusions, first solved the Navier–Stokes equation under a one-dimensional lubrication approximation using a Lagrangian method, and provided a solution describing the dynamics of the hanging drop, demonstrating that the droplet dripping interval indeed exhibits periodic, period-doubling, and chaotic behaviors. Ambravaneswaran, Wilkes, and Basaran (2002)[1–2] used the neck breakup model to verify the existence of satellite droplets, whose presence significantly alters the periodic behavior of droplet dripping intervals, and compared the error between the neck breakup model and the full two-dimensional Navier–Stokes solution, demonstrating that under lower viscosity and flow rate conditions the one-dimensional neck breakup model has sufficient accuracy and the advantage of lower computational cost. Shore and Harrison (2005)[16] found that adding polymers to the liquid can significantly delay neck contraction and breakup, lengthen the neck, and suppress the formation of satellite droplets, thereby markedly changing dripping interval behavior. The third approach is to solve the free surface equation. A general method is to process the Young–Laplace equation, determine the droplet critical volume, and then combine this with flow conditions to solve the dripping interval. Concus and Finn (1979)[4] demonstrated through

numerical integration that under quasi-static conditions a droplet always reaches a specific critical volume before detachment. Riera et al. (2002)[14] and Coulet, Mahadevan, and Riera (2004)[5] used a variational treatment of a reformulated Young–Laplace equation to show that unstable hanging-drop solutions with arbitrarily many "peaks" exist, while only a single "one-peak" solution is stable. Riera et al. (2002)[14] and Coulet, Mahadevan, and Riera (2004)[5] identified a saddle-node bifurcation as the droplet approaches the critical volume under quasi-static conditions, and described the overall dripping behavior by constructing a Lagrangian equation.

Previous experiments mainly focused on chaos analysis [17]. Martien et al. (1985)[12] first proposed an experimental measurement of droplet dripping intervals under flowing conditions, using an apparatus consisting of a spherical valve, a photoelectric gate, and a waveform processor, and plotted return maps that revealed chaotic behavior. Wu and Schelly (1989)[19] introduced a continuously adjustable flow control mechanism and high-speed data acquisition on this basis, obtaining spectra over a wide range of flow rates, discovering new quasi-periodic modes, and verifying the influence of temperature and surface tension on dripping intervals. Kiyono and Fuchikami (1999)[11] plotted return maps and bifurcation diagrams to describe chaotic behavior. Ambravaneswaran et al. (2004)[3] described the transitions among simple dripping, complex dripping, and jetting using phase diagrams[18].

1.3. Research Objectives and Research Innovations

This paper mainly models the critical volume of a droplet at the open end of a vertically downward circular thin-walled faucet and obtains an analytical solution. In the theoretical aspect, the Young–Laplace equation is used as the governing equation and is approximately solved using the perturbation method, yielding a linearized analytical solution for the hanging drop volume at any moment; convex analysis is applied to analyze the stability of the hanging drop profile, and a critical criterion is obtained based on the constraint that the profile loses stability upon reaching the critical volume; at the same time, the theoretically obtained droplet critical volume is fitted with experimental results and subjected to error analysis. In the experimental aspect, the influence of the Bond number on the magnitude of the critical volume is mainly investigated, and verification experiments are conducted. From the perspective of innovation, this paper applies the perturbation method to approximate the Young–Laplace equation for the first time. This method can provide accurate analytical solutions with relatively low computational cost, offering a new approach for calculating droplet interface profiles. Meanwhile, previous studies generally used numerical integration to determine the critical volume, whereas this paper proposes a convex-analysis-based method that can directly and effectively obtain the liquid critical volume, providing a reference for optimizing the solution process of the hanging drop volume model.

2. Theoretical Analysis

2.1. Gas–Liquid Interface Model

This paper assumes that the cross section of the open end of the faucet is horizontal, the opening direction is vertically downward, and the system satisfies radial symmetry and complete wetting. A quasi-static assumption is also adopted: under low water pressure, the change in droplet shape occurs in an almost equilibrium physical process, so all velocity-related effects on the droplet can be neglected, and the primary factors determining droplet shape are only the gravitational force acting on the droplet and surface tension. As shown in the figure, the center of the cross section of the open end of the faucet is taken as O, the vertical downward direction is taken as positive to establish the z coordinate, the horizontal rightward direction is

taken as positive to construct the r coordinate, the polar angle α is defined on the r axis to satisfy α=0, and the cylindrical coordinate system (r,α,z) is constructed.

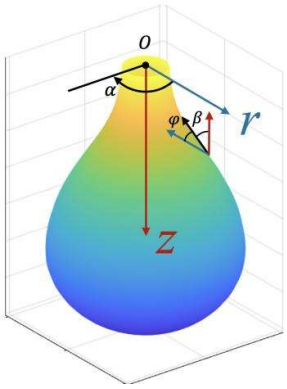

Fig. 1 Cylindrical coordinate system and related parameters

Under this coordinate system, the following relationships hold:

$$\tan\varphi=\frac{dz}{dr} \tag{1}$$

$$\sin\varphi=\frac{dz/dr}{\sqrt{1+\left(\frac{dz}{dr}\right)^2}} \tag{2}$$

$$\cos\varphi=\frac{1}{\sqrt{1+\left(\frac{dz}{dr}\right)^2}} \tag{3}$$

$$ds=\sqrt{1+\left(\frac{dz}{dr}\right)^2}\,dr \tag{4}$$

where ϕ is the angle between the tangent to the gas–liquid interface profile of the droplet and the horizontal direction.

For the hanging droplet in the faucet system, the equilibrium free surface satisfies the Young–Laplace equation:

$$\sigma\left(\frac{1}{R_1}+\frac{1}{R_2}\right)=\Delta P \tag{5}$$

where σ is the surface tension coefficient of the hanging droplet liquid; $\Delta P$is the pressure difference between the internal liquid pressure and the external atmospheric pressure at any point on the free surface; $\frac{1}{R_1}$ and $\frac{1}{R_2}$ are the two principal curvatures of the free surface at any point, among which $\frac{1}{R_1}$ is the curvature along the longitudinal section and $\frac{1}{R_2}$ is the curvature along the transverse section.

The Young–Laplace equation describes the balance among surface tension, curvature, and gas–liquid interface pressure difference at any point on the free surface of the hanging droplet. For convenience in subsequent calculations, it is rewritten in the cylindrical coordinate system (r,α,z)as:

$$\frac{1}{r}\frac{d}{dr}\frac{rdz/dr}{\sqrt{1+\left(\frac{dz}{dr}\right)^2}}-\frac{\rho gz}{\sigma}=\frac{\Delta P}{\sigma}=A \tag{6}$$

Equation (6) is the cylindrical-coordinate expression of the Young–Laplace equation for the free surface of the hanging droplet. In this expression, $\frac{1}{r}\frac{d}{dr}\frac{rdz/dr}{\sqrt{1+\left(\frac{dz}{dr}\right)^2}}$ is the curvature term, $\frac{\rho gz}{\sigma}$ is the gravitational term, and $\frac{\Delta P}{\sigma}$ is the pressure difference term. Substituting part of the terms using (2), multiplying by r, and integrating yields:

$$r\sin\varphi-\frac{\rho g}{\sigma}\int zrdr=\frac{A}{2}r^2+B \tag{7}$$

where $A=\frac{\Delta P}{\sigma}$ and B are constants of integration.

2.2. Perturbation Method Solution Procedure

It can be observed that the Young–Laplace equation is essentially a nonlinear, non-autonomous second-order ordinary differential equation with coupled constraints involving singularities and free constants. It is generally non-integrable, and mathematical techniques are required to linearize the equation and form an autonomous system that does not explicitly contain free constants. This paper applies the perturbation method for linearized solution. This method is based on the assumption that when a small parameter ε exists in the system, the solution of the problem can be expressed as a power-series expansion in ε. This approach is most suitable for flow situations in which the solution does not undergo significant variation in any local region, such as nonlinear problems under small perturbations. The specific procedure is as follows. First, nondimensionalize Eqs. (1) (7):

$$x=\frac{r}{r_1} \tag{8}$$

$$y=\frac{z}{r_1} \tag{9}$$

where r_1 is the radius of the open end of the faucet.
From this, the following expressions are obtained:

$$\sin\varphi-\frac{\rho g}{\sigma}r_1^2\int yxdx=\frac{A'}{2}x^2+B' \tag{10}$$

$$\frac{dy}{dx}=\tan\varphi=\frac{\sin\varphi}{\sqrt{\left(1-\sin^2\varphi\right)}} \tag{11}$$

where $A^{'}=Ar_1$ and $B^{'}$ are dimensionless parameters; $\frac{\rho g}{\sigma}r_1^2=\varepsilon$ is the Bond number, representing the relative magnitude of gravitational force and surface tension.

Let ε be the perturbation parameter, and expand several variables with respect to this parameter:

$$\left.\begin{array}{l} y=y_0+\varepsilon y_1 \\ \varphi=\varphi_0+\varepsilon\varphi_1 \\ A^{'}=A_0^{'}+\varepsilon A_1^{'} \\ B^{'}=B_0^{'}+\varepsilon B_1^{'} \end{array}\right\} \tag{12}$$

Substituting Eq. (12) into the original Equation (10-11) by order yields the zeroth-order expansion results:

$$\frac{\mathrm{d}y_0}{\mathrm{d}x}=\tan\varphi_0=\frac{\sin\varphi_0}{\sqrt{\left(1-\sin^2\varphi_0\right)}} \tag{13}$$

$$x\sin\varphi_0=\frac{A_0^{'}}{2}x^2+B_0^{'} \tag{14}$$

and the first-order expansion results:

$$\varphi_1 x\cos\varphi_0+\int_0^x y_0\,ndn=\frac{A_1^{'}}{2}x^2+B_1^{'} \tag{15}$$

$$\frac{dy_1}{dx}=\frac{\varphi_1}{\cos^2\varphi_0} \tag{16}$$

where $n$is the dummy variable used in the zeroth-order profile integration. In this way, the linearized expressions of the original equation are obtained, and analytical solutions can be found by performing separate transformations. Terms of second order and higher are neglected to reduce computational effort. The influence of higher-order terms on volume under different Bond numbers is as follows.

(1) Zeroth-Order Expansion

The zeroth-order result excludes the gravitational term, and its physical meaning corresponds to the droplet shape in the absence of gravitational perturbation. The solution procedure is presented below. For the zeroth-order expansion equations:

$$\frac{\mathrm{d}y_0}{\mathrm{d}x}=\tan\varphi_0=\frac{\sin\varphi_0}{\sqrt{\left(1-\sin^2\varphi_0\right)}} \tag{17}$$

$$x\sin\varphi_0=\frac{A_0^{'}}{2}x^2+B_0^{'} \tag{18}$$

The boundary conditions are:

$$\begin{cases} x=0,\varphi_0=0 \\ x=1,\varphi_0=\theta \quad y_0=0 \end{cases} \tag{19}$$

Substituting (19) into (18), and considering the coordinate position of the droplet free surface, yields:

$$dy_0=\frac{\sin(\theta)x}{\sqrt{1-\sin^2(\theta)x^2}}dx \tag{20}$$

Integrating Eq. (21) for any $\theta\notin\{0,\pi\}$ gives:

$$\begin{aligned} y_0&=-\frac{1}{2\sin\theta}\int\sqrt{u}du=-\frac{1}{\sin\theta}\sqrt{u}+C \\ &=-\frac{1}{\sin\theta}\sqrt{1-\sin^2\theta x^2}+C \end{aligned} \tag{21}$$

For the constant C in Eq. (21), substituting into the boundary condition $*y_0(1)=0$ determines the expression as:

$$C=\frac{\cos\theta}{\sin\theta}=\cot\theta \tag{22}$$

Substituting back and simplifying yields the zeroth-order free surface profile of the droplet:

$$y_0(x)=\cot\theta-\frac{\sqrt{1-\sin^2\theta x^2}}{\sin\theta} \tag{23}$$

This expression describes the shape of the droplet free surface profile at any x coordinate without gravitational perturbation.

(2) First-Order Expansion

The first-order term is used to represent the influence of gravity on the droplet shape. The solution procedure is as follows. The first-order expansion equations are:

$$\varphi_1 x\cos\varphi_0+\int_0^x y_0(n)ndn=\frac{A_1^{'}}{2}x^2+B_1^{'} \tag{24}$$

$$\frac{dy_1}{dx}=\frac{\varphi_1}{\cos^2\varphi_0} \tag{25}$$

Substituting the boundary conditions:

$$x=0,\varphi_1=0 \tag{26}$$
$$x=1,\varphi_1=0,y_1=0$$

yields the first-order parameter expressions:

$$B_1^{'}=\int_0^0 y_0\, ndn$$
$$A_1^{'}=2\left(\int_0^1 y_0\, ndn\right)-B_1^{'}=2I_0 \tag{27}$$
$$\varphi_1(x)=\frac{-I(1)x^2+I(x)}{x\sqrt{1-\sin^2\theta x^2}}$$

where $I_0=\frac{V_0}{2\pi}$. Substituting these parameters back into Eqs. (24-25) and integrating yields:

$$y_1=\int_0^x \frac{V_0n^2-V(n)}{n\cos^3\varphi_0}dn \tag{28}$$

2.3. Stability Analysis

During droplet growth, the stability of the hanging state is a critical issue. When the droplet grows to a certain volume, the gravitational force exceeds the balancing surface tension, and the droplet can no longer remain stably suspended at the faucet. Its profile and distribution evolve rapidly without external disturbance, eventually detaching from the faucet. This process is referred to as droplet instability, and the critical volume at instability is a key focus of study.

As discussed in the previous section, during droplet growth there exists a one-to-one correspondence between droplet volume and the actual contact angle, and the contact angle is the key factor affecting stability[13]. As shown in the figure:

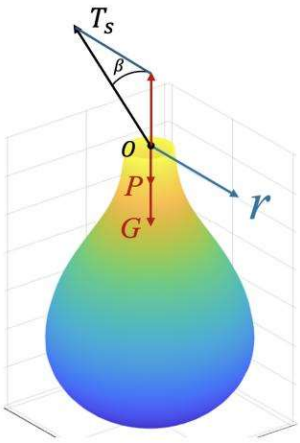

Fig. 2 Force balance diagram of the hanging droplet

At the faucet outlet, consider a cross section perpendicular to the z-axis. The droplet portion below this section is in force equilibrium when stable, meaning that the gravitational force acting on the droplet is balanced by the vertical component of surface tension along the circular boundary of the section. The equilibrium equation can be written as

$$2\sigma\pi x(0)\cos\beta - P\pi x(0)^2 = G \tag{29}$$

where β is the angle between the droplet surface and the section, and G is the gravitational force acting on the droplet at the faucet opening.

When the droplet volume increases further, the gravitational force increases. Since the droplet radius at the faucet outlet is fixed, to restore equilibrium β shifts toward 90 degrees. Thus, regardless of whether the intrinsic contact angle of the droplet (or the initial contact angle during droplet growth) is greater than or less than 90 degrees, the actual contact angle evolves toward 90 degrees during growth. When $\beta=\pi/2$, the vertical component of surface tension reaches its maximum. If the volume increases further, surface tension can no longer balance gravity, and instability occurs. This condition represents a critical solution to the droplet instability problem.

On this basis, the Young–Laplace equation used here exhibits the properties of a convex function. The gravitational term as a function of droplet curvature is convex. According to convex function theory, such a function has one and only one solution to a given critical problem within its domain. Therefore, the obtained solution can be regarded as the unique critical solution to this problem.

3. Experiment

The purpose of the experiments in this paper is to verify the correctness and accuracy of the theoretical analytical results. In this chapter, a controlled-variable experiment with respect to faucet diameter is established to investigate the influence of the Bond number on the droplet critical volume. A propulsion device is used to simulate a constant upstream pressure, forcing water out from the open end of the faucet. The critical droplet volume in the experiment is obtained through image capture, and is fitted with the theoretical solution to evaluate the error of the theoretical prediction.

3.1. Experimental Apparatus

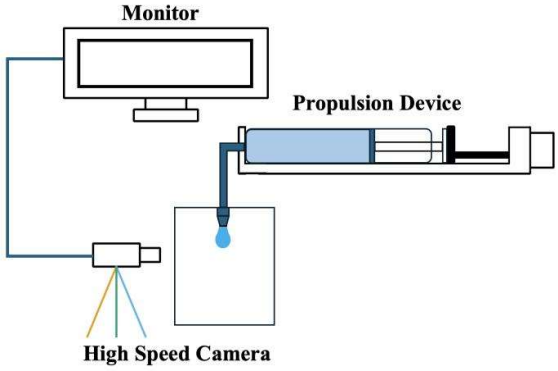

Fig. 3 Schematic diagram of the experimental apparatus

As shown in the figure, the experimental apparatus is divided into three parts: the propulsion mechanism, the imaging device, and the computation and analysis equipment. The propulsion device is the main component forming the faucet system and includes: a horizontally mounted pusher with a minimum propulsion speed of 0.01 mm/s and a maximum propulsion speed of

3.0 mm/s, controlled by a programmed microcontroller; a 50 ml Luer syringe with an inner wall radius of 3 cm; six faucets with different inner diameters, whose numbering corresponds to diameter values as shown in the table, made of PS; and a Luer elbow connector used to connect the horizontally placed propulsion mechanism to the faucet. The imaging device records the physical process of droplet dripping and includes a high-speed camera with a frame rate of 815 fps and a connected recording device with unrestricted output and continuous storage. The computation and analysis equipment processes images to determine the critical volume, and the image-processing software Fiji is used.

Table 1. Faucet Inner Diameters

Number	Faucet Inner Diameter (mm)
1	0.99
2	1.58
3	2.46
4	2.96
5	3.94
6	5.42

3.2. Experimental Method

The experimental procedure is as follows. First, the flow rate is calculated using the geometric parameters of the syringe and the propulsion speed. A sufficiently small propulsion speed is selected to produce a sufficiently small flow rate, simulating the quasi-static condition assumed in the theory. The flow rate used in the experiment is $1.5^2\pi 510^{-2}=0.353ml^3/s$. Next, the six faucets with different inner diameters are sequentially mounted onto the syringe and the system is adjusted to ensure complete wetting of the faucet and absence of air bubbles in the syringe. Each faucet is then tested in sequence: after activating the propulsion device, droplets are allowed to drip while high-speed imaging is performed with the frame rate and storage settings described earlier, and ten droplets are recorded for each faucet. Finally, images corresponding to the critical droplet condition are selected and processed using Fiji to obtain experimental data, and the average value is calculated.

3.3. Experimental Apparatus

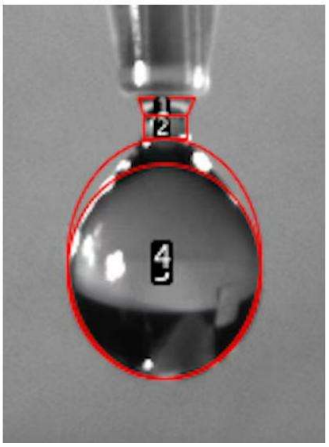

Fig. 4 Schematic diagram of the volume calculation method

The above procedure minimizes disturbances and errors while maintaining a single controlled variable r. It is necessary to clarify the image selection method. According to theory, when the hanging droplet contact angle reaches $\varphi=\frac{\pi}{2}$, the critical volume is achieved, and any disturbance

thereafter causes instability and detachment. In practice, due to various errors such as imperfect vertical alignment of the faucet opening, frame rate limitations, and parallax, it is difficult to identify the exact moment when the contact angle reaches $\frac{\pi}{2}$. Moreover, since only side-view images of the droplet can be captured, using the droplet shape at the moment when the contact angle reaches $\frac{\pi}{2}$ makes volume measurement and calculation extremely difficult. Therefore, as shown in the figure, the droplet volume at the instant of detachment is used as the experimental critical volume [20]. This approach simplifies calculation by approximating the contour as geometric shapes and allows high-precision contour reconstruction within a short processing time. After image processing in Fiji, Python is used to identify the necessary physical quantities to obtain the critical volume.

3.4. Experimental Results and Discussion

Based on the above experimental procedure, the experimental data are obtained as shown in the figure. The second column lists the theoretical analytical results, the third column lists the experimental data, the fourth column presents the experimental error, and the final column shows the comparison difference between theory and experiment.

It can be observed that the experimental data contain inherent errors. These errors arise from two main sources: systematic errors, including occasional vibration of the propulsion device and non-vertical alignment of the faucet opening; and random errors, including the possibility that high-speed camera frames do not exactly capture the detachment instant, contour measurement inaccuracies during image processing, and precision limitations when Python identifies required physical quantities.

At the same time, the theoretical model shows good agreement with experimental data. The difference relative to experimental results ranges from 2% to 12%. Considering the limitations of experimental equipment and the uncertainty in volume estimation, this level of accuracy is acceptable. The experiment confirms that faucet diameter is positively correlated with the droplet critical volume.

Table 2. Theory and Experiment Results

Number	Theo. (μl)	Exp. (μl)	Err. Analysis	Theo. & Exp. Comparison
1	4.7	4.55	1.36%	3.2%
2	8.1	7.59	1.41%	6.2%
3	14.2	12.46	0.19%	12%
4	40.1	38.57	4.24%	3.8%
5	47.2	50.96	1.58%	7.3%
6	53.1	54.3	1.34%	2%

Considering the errors from experimental equipment and volume estimation, the achieved precision is acceptable. The experiment verifies that faucet diameter is related to droplet critical volume and exhibits a positive correlation.

In addition, experiments are conducted to investigate the influence of the initial contact angle on the critical volume. The results, shown in the corresponding table, indicate that the variation in critical volume under different initial contact angles is very small, demonstrating that the critical volume is independent of contact angle. This conclusion can also be derived theoretically. Since the critical contact angle is fixed, the nondimensional droplet profile is unique for a given contact angle and Bond number, and the only parameter influencing droplet volume is the faucet radius.

4. Conclusion

This paper employs an analytical method based on the perturbation method for the Young–Laplace equation to compute the profile and critical volume of a hanging droplet at the outlet of a vertically oriented thin-walled faucet. An approximate analytical solution describing the variation of droplet morphology with Bond number is obtained, achieving high accuracy while significantly reducing computational cost. Through convex analysis, a unique critical solution condition is established. Experimental validation is carried out using high-speed imaging with six different faucet diameters, confirming the theoretical results, with deviations between theory and experiment controlled within 2–12%. Both theory and experiment indicate that the critical volume is independent of the intrinsic contact angle of the liquid, while increasing monotonically with faucet radius. Future work may be extended in several directions: introducing dynamic pressure into the existing quasi-static framework to reveal droplet morphology under higher flow-rate conditions; extending the method to faucets without radial symmetry; incorporating more rigorous stability analysis approaches such as regular modal stability analysis; and applying the analytical framework to practical systems such as inkjet printing, microfluidics, and propulsion, including extensions to complex nozzle geometries and multiphase flow systems.

References

[1] Ambravaneswaran, B., Phillips, S. D., and Basaran, O. A., "Theoretical analysis of a dripping faucet," Phys. Rev. Lett. 85 (2000).

[2] Ambravaneswaran, B., Wilkes, E. D., and Basaran, O. A., "Drop formation from a capillary tube: Comparison of one-dimensional and two-dimensional analyses and occurrence of satellite drops," Phys. Fluids 14 (2002).

[3] Ambravaneswaran, B., Subramani, H. J., Phillips, S. D., and Basaran, O. A., "Dripping-jetting transitions in a dripping faucet," Phys. Rev. Lett. 93 (2004).

[4] Concus, P. and Finn, R., "The shape of a pendent liquid drop," Phil. Trans. R. Soc. Lond. A 292, 307–340 (1979).

[5] Coulet, P., Mahadevan, L., and Riera, C. S., "Hydrodynamical models for the chaotic dripping faucet," J. Fluid Mech. 526, 1–17 (2004).

[6] D'Innocenzo, A. and Renna, L., "Analytical solution of the dripping faucet dynamics," Phys. Lett. A 220, 75–80 (1996).

[7] Eggers, J., "Nonlinear dynamics and breakup of free-surface flows," Rev. Mod. Phys. 69, 865–929 (1997).

[8] Eggers, J. and Dupont, T. F., "Drop formation in a one-dimensional approximation of the Navier–Stokes equation," J. Fluid Mech. 262, 205–221 (1994).

[9] Fuchikami, N., Ishioka, S., and Kiyono, K., "Simulation of a dripping faucet," J. Phys. Soc. Jpn. 68, 1185–1196 (1999).

[10] Harkins, W. D. and Brown, F. E., "The determination of surface tension (free surface energy), and the weight of falling drops: The surface tension of water and benzene by the capillary height method," J. Am. Chem. Soc. 41, 499–524 (1918).

[11] Kiyono, K. and Fuchikami, N., "Dripping faucet dynamics by an improved mass-spring model," J. Phys. Soc. Jpn. 68, 3259–3270 (1999).

[12] Martien, P., Pope, S. C., Scott, P. L., and Shaw, R. S., "The chaotic behavior of the leaky faucet," Phys. Lett. A 110, 399–404 (1985).

[13] Padday, J. F. and Pitt, A. R., "The stability of axisymmetric menisci," Phil. Trans. R. Soc. Lond. A (1973).

[14] Riera, C. S. and Risler, E., "Axisymmetric capillary surfaces as a dynamical system," Nonlinearity 15, 1843–1879 (2002).

[15] Sánchez-Ortiz, G. I. and Salas-Brito, A. L., “Strange attractors in a relaxation oscillator model for the dripping water faucet,” Phys. Lett. A 203, 300–311 (1995).

[16] Shore, H. J. and Harrison, G. M., “The effect of added polymers on the formation of drops ejected from a nozzle,” Phys. Fluids 17 (2005).

[17] Smith, S. W. J. and Moss, H., “Experiments with mercury jets,” Proc. R. Soc. Lond. A 93, 373–393 (1917).

[18] Subramani, H. J., Yeoh, H. K., Suryo, R., Xu, Q., Ambravaneswaran, B., and Basaran, O. A., “Simplicity and complexity in a dripping faucet,” Phys. Fluids 18 (2006).

[19] Wu, X. and Schelly, Z. A., “The effect of surface tension and temperature on the nonlinear dynamics of the dripping faucet,” Physica D 40, 433–443 (1989).

[20] Yildirim, O. E., Xu, Q., and Basaran, O. A., “Analysis of the drop weight method,” Phys. Fluids 17 (2005).